



Science Arts & Métiers (SAM)

is an open access repository that collects the work of Arts et Métiers Institute of Technology researchers and makes it freely available over the web where possible.

This is an author-deposited version published in: <https://sam.ensam.eu>
Handle ID: <http://hdl.handle.net/10985/11774>

To cite this version :

Vincent COGNET, Sylvain COURRECH DU PONT, Ivan DOBREV, Fawaz MASSOUH, Benjamin THIRIA - Bioinspired turbine blades offer new perspectives for wind energy - Proceedings of the Royal Society A: Mathematical, Physical and Engineering Sciences - Vol. 473, n°2198, p.2449-1065 - 2017

Any correspondence concerning this service should be sent to the repository

Administrator : scienceouverte@ensam.eu



Bioinspired turbine blades offer new perspectives for wind energy

V. Cagnet¹, S. Courrech du Pont², I. Dobrev³,
F. Massouh³ and B. Thiria¹

Subject Areas:

energy, power and energy systems,
fluid mechanics

Keywords:

wind energy, bio-inspiration, reconfiguration
mechanisms

Author for correspondence:

Vincent Cagnet

e-mail: vincent.cagnet@espci.fr

¹Laboratoire de Physique et Mécanique des Milieux Hétérogènes (PMMH), UMR CNRS 7636, ESPCI Paris, PSL Research University, Sorbonne Université, Univ. Paris Diderot, 10 rue Vauquelin 75005 Paris, France

²Laboratoire Matière et Systèmes Complexes, UMR CNRS 7057, Sorbonne Paris Cité. Univ. Paris Diderot, Bât. Condorcet, 10 rue Alice Domon & Léonie Duquet, 75013 Paris, France

³Laboratoire de Dynamique des Fluides, École Nationale Supérieure des Arts et Métiers-ParisTech, 151, boulevard de l'hôpital, Paris, France

Wind energy is becoming a significant alternative solution for future energy production. Modern turbines now benefit from engineering expertise, and a large variety of different models exists, depending on the context and needs. However, classical wind turbines are designed to operate within a narrow zone centred around their optimal working point. This limitation prevents the use of sites with variable wind to harvest energy, involving significant energetic and economic losses. Here, we present a new type of bioinspired wind turbine using elastic blades, which passively deform through the air loading and centrifugal effects. This work is inspired from recent studies on insect flight and plant reconfiguration, which show the ability of elastic wings or leaves to adapt to the wind conditions and thereby to optimize performance. We show that in the context of energy production, the reconfiguration of the elastic blades significantly extends the range of operating regimes using only passive, non-consuming mechanisms. The versatility of the new turbine model leads to a

large increase of the converted energy rate, up to 35%. The fluid/elasticity mechanisms involved for the reconfiguration capability of the new blades are analysed in detail, using experimental observations and modelling.

1. introduction

To a large extent, the global energy demand for the next decades will be based on renewable energies. Recent scenarios for 2050 reported by the International Energy Agency (IEA) or the Organization for Economic Co-operation and Development (OECD) predict that wind energy will represent 12% of the electricity produced on the planet. Today, the total amount produced by wind turbines covers less than 4%, meaning that the main effort in developing wind energy is still to come. The challenges are of course to reduce the turbine cost and increase the farm size; another one, though, is to overcome technological limitations of the turbines themselves and provide sustainable technological solutions.

Current wind turbines are efficient at specific working points [1]. This limitation is mainly due to the fact that for a given blade design (setting local angles of attack and aerodynamic coefficients along the blade), the turbine reaches its best performance over a narrow band of oncoming wind speeds and turbine loads [1,2].

As a consequence, the energy conversion is poor when the turbine is working far from its operating regime. For current installation, this difficulty is generally overcome either by seeking sites with stable and constant head wind or by introducing active motorized controls of blade pitch angle [2] or active trailing edge flaps [3]. Nevertheless, a large amount of potential available wind energy is not converted by the turbines, leading to a significant energetic and economic losses. This lack of versatility limits the development of small or middle-sized turbine models and the expansion of short supply chains.

This work introduces a solution to this technological limitation, using flexible blades inspired by the flapping flight of insects and reconfiguration of plants. Slender elastic structures, such as wings or leaves, adjust the torque exerted by the fluid pressure when bending through the action of the incoming wind, changing the balance between external mechanical loads [4–6]. Plants bend during wind conditions, which reduces drag and avoids damage [7–9]. Insects, on the other hand, use this ability to change the direction of the pressure forces to improve thrust production, without extra input energy [10–12]. Along the same line of thought, flexible blades can be implemented on wind turbines.

Blade flexibility is currently a centre of attention in the turbine community. The principal concern has been the structural instability of large size turbines operating at high tip speed ratios. The main goal of these works has been to include blade flexibility into models and simulations to give accurate predictions of the blade bending and flutter threshold [2,13,14]. On the other hand, blade flexibility has also been perceived as a way to improve the performance of the rotor. Several numerical studies have addressed chordwise bending of the blade through the action of the aerodynamic load and have shown that performance could be increased in specific cases [15–21], but did not consider the blade pitch angle as a key parameter. This parameter is, however, crucial for flexible blades because the main property of flexibility is to allow the pitch angle to dynamically adapt to the wind forcing and extracted power. We propose an experimental and theoretical study covering a relevant range of the parameter space.

We show that the most notable feature of the blade reconfiguration capability is to keep the mechanical system efficient away from the optimal operating point (in the case of wind conditions, which are below or above the nominal speed, for instance). This crucial feature can significantly extend the performance range of wind turbines beyond their specific working regime. Our experimental results show an increase in potential energy production up to 35%, which is obtained using passive, non-consuming mechanisms, from the reservoir of energy available at non-nominal wind conditions.

Because a wind turbine design is a multiple entry problem (number of blades, profiles, orientation, inclination, type of rotor, size, wind regimes, etc.), the present analysis is intentionally conducted on a reduced mechanical system. The model is three-bladed and the blade profiles consist of non-twisted flat membranes of constant thickness, of length $L = 10$ cm and chord $W = 4.5$ cm, clamped to a rigid rod. Membranes are able to deform in the chordwise direction as shown in figure 1. The rotor stands $H = 20$ cm above the ground; the radius of the rotor, measured from centre to blade tip, is $R = 14.6$ cm.

The flexible part of the blade (of width $w = 3.5$ cm) is made from PET (polyethylene terephthalate) sheets, with a specific rigidity B that can be varied using different thicknesses. We focused on two characteristic flexible cases: the first, referred to as semi-flexible F_1 and a second, referred to as very flexible F_2 , corresponding to bending modulus B_1 and B_2 , respectively (details can be found in the Methods section). For the very soft case F_2 , blades may flutter at high wind velocities. However, the working ranges of the turbine are far from the fluttering threshold. Both elastic cases must be compared with rigid blades (referred to as RB), printed in synthetic resin.

For the three configurations (RB, F_1 and F_2), we measured the angular frequency Ω as a function of the headwind velocity U , the resistive torque C (mimicking the extraction of energy converted to electricity, see [1]), along with the pitch angle of the blade θ_0 .

The power coefficient C_P of the turbine can be estimated comparing the power absorbed by the resistive torque $C\Omega$, to the total available wind power, defined as the unperturbed wind kinetic energy flux through the surface swept by the turbine $\frac{1}{2}\rho U^3 \pi R^2$

$$C_P = \frac{C\Omega}{(1/2)\rho U^3 \pi R^2} = C^* \lambda. \quad (2.1)$$

The second expression of C_P introduces the characteristic speed ratio $\lambda = R\Omega/U$ between the turbine and the wind velocities, and the expression of the dimensionless torque $C^* = C/(0.5\rho U^2 \pi R^3)$. The ratio λ intrinsically depends on the local apparent angle of attack β through the following geometrical relation (figure 1)

$$\beta = \arctan\left(\frac{1}{\lambda}\right) - \theta_0. \quad (2.2)$$

For a given set of parameters (θ_0, B) , an efficiency map of C_P can be constructed, varying U and C independently. Figure 2 shows maps for the three different sets of blades (RB, F_1 , F_2) obtained for a value of the pitch angle $\theta_0 = 30^\circ$, close to the optimum pitch angle θ_0^{opt} for which the efficiency C_P is maximum over the experimental ranges of U and C . These maps show typical responses of the turbine to imposed parameters, showing an optimal zone of performance. For a given U (resp. a given C), one can observe that the efficiency goes through a maximum when varying C (resp. U). Indeed, when looking at a $C_P(C)$ profile taken at a fixed U , C_P will take its value between two limiting cases of $C_P = 0$, corresponding to no load ($C = 0$) and a strong load preventing the rotor from running ($\Omega = 0$). We observe the same behaviour for a $C_P(U)$ profile taken at a fixed C . The lower limit $C_P = 0$ is directly set by $U = 0$. The second, though, is caused by the alignment of the apparent angle of attack β with the blade due to an excessive rotation rate, setting the aerodynamic torque applied on the blade close to zero [1].

Comparing the three cases of rigidity, we see a strong effect of the blade stiffness. The working range obtained for blades F_1 appears wider than that obtained for the rigid and F_2 blades. This suggests an optimum depending on blade deformation, which increases the versatility of the turbine. To quantify this observation, we extract from these measurements three representative quantities related to the turbine efficiency. For a fixed wind velocity, varying both the resistive torque C and pitch angle θ_0 , we determined C_P^{max} , the maximum efficiency, I_{50} , the integral of C_P above 50 % of C_P^{max} and I_{100} , the total integrated efficiency. I_{50} is probably the most relevant quantity for energy purposes, as it gives weight to the vicinity of the optimum working point.

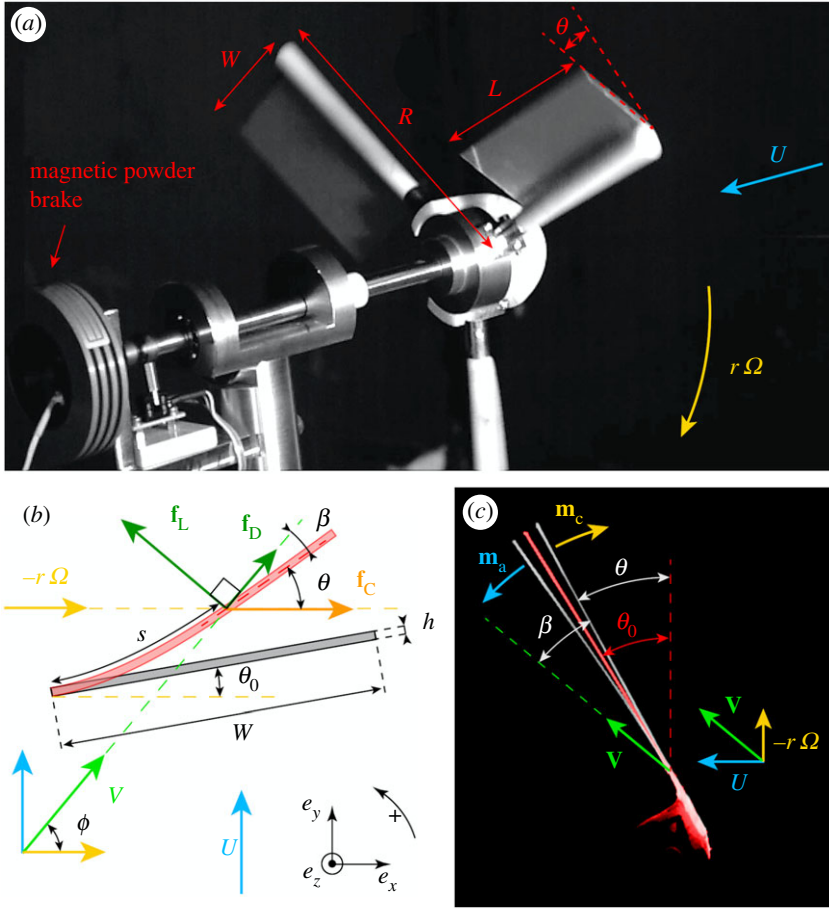


Figure 1. (a) Three-bladed turbine model used in this work. (b) Sketch of a blade section in the rotating frame of reference, showing symbols and notation. During the operating regime, the blade is subjected to the aerodynamic force (decomposed into lift \mathbf{f}_L and drag \mathbf{f}_D), which tends to fold the blade through the action of the torque \mathbf{m}_a , and the centrifugal force \mathbf{f}_c , which conversely tends to align the blade with the rotation plane due to the torque \mathbf{m}_c exerted in the opposite direction. As a result, the blade bends, which modifies the angle of attack β between the apparent wind \mathbf{V} and the blade and θ , the angle between the blade and the plane of rotation. (c) Bent elastic blades for three characteristic values of the speed ratio λ measured at the tip blade. The red profile shows the reference configuration ($\lambda = 0$, $\theta_0 = 28^\circ$). The two white profiles show the bent blades for ($\lambda = 0.25$, $\theta = 30.8^\circ$) and ($\lambda = 2.35$, $\theta = 25.3^\circ$).

Figure 3 shows these three quantities as functions of the blade pitch angle and compares rigid (RB, black circles), semi-flexible (F_1 , red squares) and very flexible blades (F_2 , green triangles) for three different wind speeds. Whatever the value of the pitch angle θ_0 or wind speed, the elastic case F_1 always gives better results than its rigid counterpart. This is true when considering C_P^{\max} , I_{50} or I_{100} . C_P^{\max} increases by 2 to 5% over the whole range of the parameters space. However, the most significant effect is observed on the integrated quantities. The increase over the full working range (I_{100}) goes from 10 to 20% and I_{50} , the integrated efficiency in the vicinity of the optimum working point, increases significantly by 15 to 35%. One can also note the presence of optima with respect to the pitch angle θ_0 . We see that this optimum is sharper for rigid blades than for F_1 blades, suggesting that the performance of the wind turbine is less dependent on an accurate tuning of the pitch angle when the blades are allowed to bend. In addition, the value of θ_0^{opt} appears to depend on the wind velocity. More generally, the optimum value of the pitch angle depends on the turbine working regime [1]. We shall see that this angle plays an important role

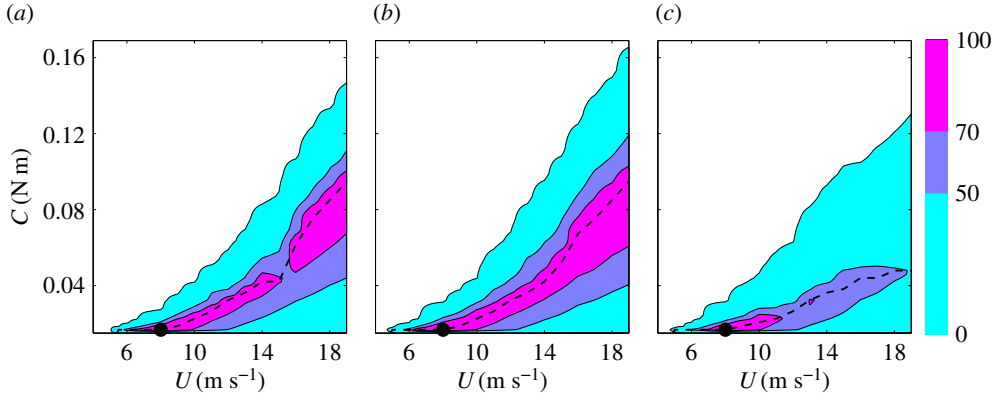


Figure 2. Efficiency maps C_p as a function of the headwind velocity U and the resistive torque C for a pitch angle $\theta_0 = 30^\circ$, for, (a) the case RB (reference), (b) F_1 and (c) F_2 . The efficiency C_p is expressed as a percentage of the maximum efficiency reached at $\theta_0 = 30^\circ$ for the rigid case ($C_p^{\max} = 0.0936$). Resolutions for both U and C are respectively 1 m s^{-1} and 8 mN m . As can be observed, the case F_1 shows an extension of the working domain of the turbine and of its high-efficiency range (above 50% of C_p^{\max}). Case F_2 , though, shows a strong decrease of the performance compared with its rigid counterpart.

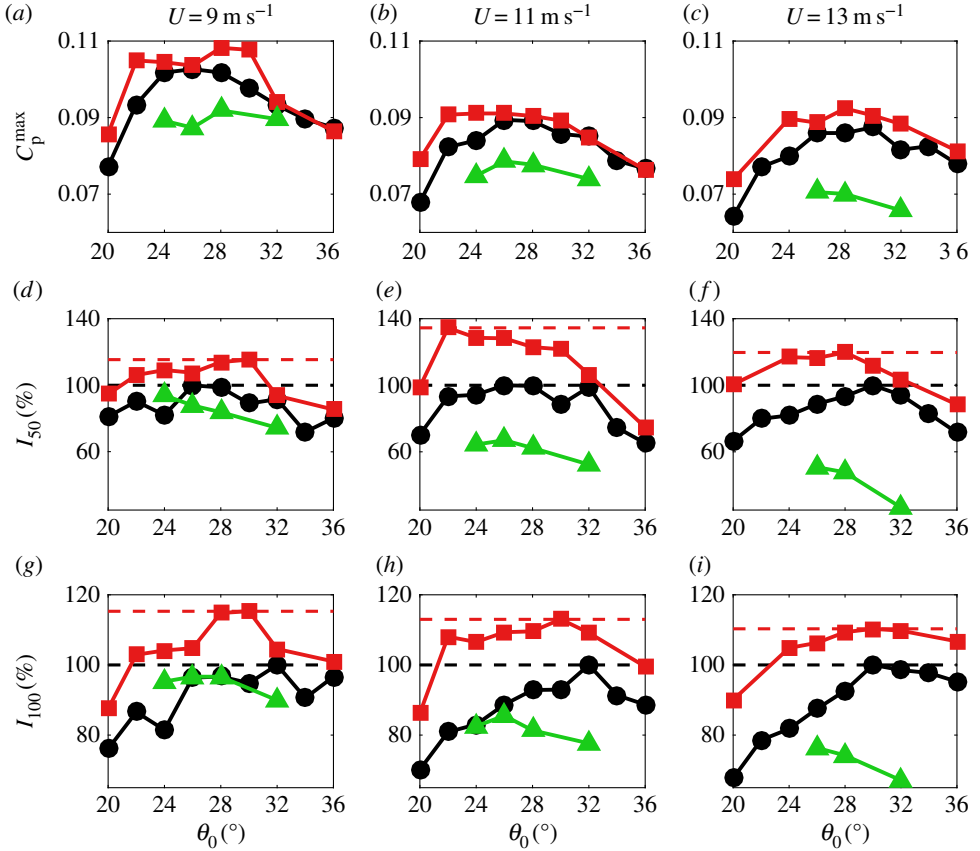


Figure 3. Representative quantities of the turbine efficiency from the experimental curves $C_p(C)$ as a function of the pitch angle θ_0 , at different headwind speeds U for the three cases of rigidity studied above (rigid, black circles, F_1 , red squares and F_2 , green triangles). (a–c) C_p^{\max} , (d–f) I_{50} (the integral of C_p above 50% of C_p^{\max}) and (g–i) I_{100} (integral of the curve $C_p(C)$ over the full working range). Each integral is normalized by the maximum integral obtained with the rigid blade turbine at a given velocity U .

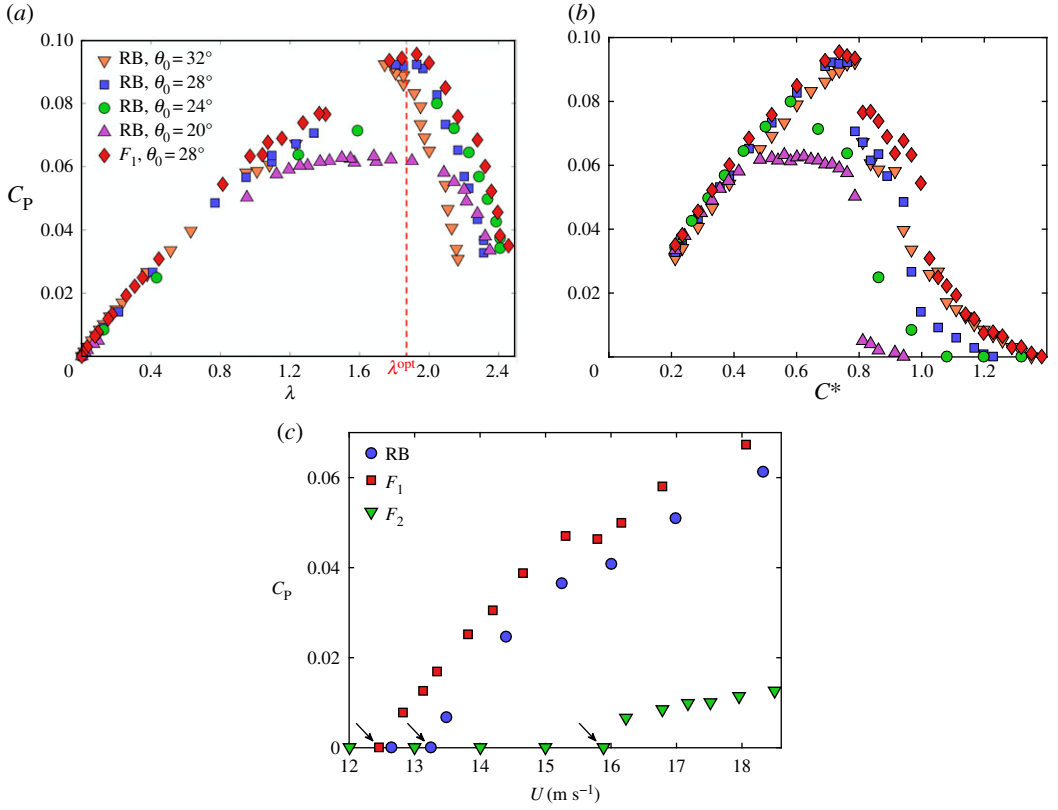


Figure 4. Efficiency curves C_p as a function of (a) λ and (b) C^* measured at the best pitch angle ($\theta_0 = 28^\circ$) for the F_1 blade, which should be compared to efficiency curves of rigid blades (RB) measured at different pitch angles ($\theta_0 = 20^\circ, 24^\circ, 28^\circ$ and 32°). Measurements are carried out varying C for a fixed headwind speed $U = 13 \text{ m s}^{-1}$. Uncertainties are due to the precision of the measuring devices and are of the order of magnitude of the markers. (c) Efficiency curves as a function of the headwind speed U , for a pitch angle $\theta_0 = 30^\circ$, for systems RB, F_1 and F_2 . The resistive torque is set to a constant value: $C = 90.9 \text{ mN m}$. A moderate blade flexibility allows an early start of the wind turbine rotation.

for the performance of the whole mechanical system. This point is addressed in detail further in the text.

Figure 4a shows the classical efficiency curve C_p plotted as a function of the speed ratio λ for F_1 blades at the optimum pitch angle $\theta_0 = 28^\circ$. It is compared to the efficiency curves of the rigid blades obtained at different pitch angles $\theta_0 = 32^\circ, 28^\circ, 24^\circ$ and 20° . As already noted in figure 3, the efficiency of the flexible system F_1 overcomes all the represented rigid counterparts. This is especially notable in the nearness and beyond the maximum efficiency $C_{p_{max}}$. However, depending on the range of λ , the performance of the F_1 case can always be compared locally to one of the RB efficiency curves displayed on figure 4a. For instance, the maximum efficiency of the F_1 case is accurately reproduced by the RB case at pitch angle $\theta_0 = 28^\circ$. The upper range of λ ($2.1 \lesssim \lambda \lesssim 2.5$), though, is close to the RB case at pitch angle $\theta_0 = 24^\circ$. Although less obvious, this property holds for the lower range of λ observed in figure 4 where the $C_p(\lambda)$ curves of the different blade systems tend to overlap. For this specific range ($0 \lesssim \lambda \lesssim 0.9$), which corresponds to small wind velocities U and/or large resistive torques C , the effect of the pitch angle on the efficiency is better illustrated when plotting C_p as a function of C^* for a fixed U , as displayed in figure 4b. For large C^* (i.e. $\lambda \lesssim 0.9$), we see that the F_1 efficiency curve is this time better reproduced by the RB case at a pitch angle $\theta_0 = 32^\circ$. F_1 flexible blades at $\theta_0 = 28^\circ$ improve the efficiency of the optimal rigid case (which is also obtained for θ_0 about 28°) over the whole working range of the turbine (i.e. C_p is increased in both high and low λ regions).

Thus, over the whole range of λ , the flexible blade system F_1 with $\theta_0 = 28^\circ$ enables efficiency values of rigid systems with θ_0 ranging from 32° (small λ) to 24° (large λ) to be obtained. Indeed, the flexible blade passively adapts the apparent pitch angle to the functioning regime, improving the efficiency. The range of pitch angles $24 \leq \theta_0 < 32^\circ$, for which rigid blade systems sweep the efficiency of F_1 system with $\theta_0 = 28^\circ$ is consistent with the blade deformation when the turbine is operating. At the blade tip, we measured a modified pitch angle $\theta = 30.8^\circ$ when $\lambda = 0.25$ and $\theta = 25.3^\circ$ when $\lambda = 2.35$ (figure 1). It is worth noting that small deformations produce large effects on the performance. It can also be observed that rigid blades at pitch angle $\theta_0 = 20^\circ$ (filled purple triangles) are always surpassed by the F_1 case at $\theta_0 = 28^\circ$ or by the RB case when $24^\circ \leq \theta_0 \leq 32^\circ$. An excessively flexible blade could give apparent pitch angles beyond the range $24^\circ \leq \theta_0 \leq 32^\circ$, leading to poor performances (see again figure 3).

Moreover, it should be noted that the increase of the pitch angle for small values of λ also favours the starting of the turbine (i.e. plays on the critical wind speed at which the turbine starts operating). This point is illustrated in figure 4c where C_P is plotted as a function of the headwind speed U , at pitch angle $\theta_0 = 30^\circ$. Initially at rest, the turbine with F_1 blades starts rotating before the two other cases RB and F_2 .

3. Discussion

The following discussion aims at understanding the fluid/elasticity mechanisms governing the performance enhancement. As seen, the efficiency curve is extremely sensitive to the tuning of the pitch angle. For our experiment, figure 5a shows the evolution of the measured optimal pitch angle θ_0^{opt} as a function of the speed ratio λ for the rigid blades model. This optimal angle $\theta_0^{\text{opt}}(\lambda)$ is evaluated by maximizing C_P for each value of λ included in the range of pitch angle $[0, \pi/2]$. As can be noted, $\theta_0^{\text{opt}}(\lambda)$ is a decreasing function of λ , meaning that the turbine should continuously adapt its pitch angle to any changing wind condition in order to maintain an optimal operating regime. This problem is already known by manufacturers and taken into account in some current turbine models using an active pitch control [2,22]. This feature may be understood by means of a simple mechanical model of a rigid bladed turbine. In the stationary regime, the equilibrium is defined as the balance between the total aerodynamical torque exerted on the blades \mathbf{M}_a and the resistive torque $C\mathbf{e}_z$. \mathbf{M}_a is calculated using a two-dimensional approach, integrating the local pressure load on the blade section over the chord length. The pressure force \mathbf{f} is decomposed into lift and drag forces as $\mathbf{f} = \mathbf{f}_L + \mathbf{f}_D$ with $|\mathbf{f}_L| = (\rho/2)C_L V^2 W$ and $|\mathbf{f}_D| = (\rho/2)C_D V^2 W$, where \mathbf{V} is the apparent local wind speed defined as $\mathbf{V}(r, s) = U\mathbf{e}_y + r\Omega\mathbf{e}_x$, i.e. $V(r, s) = U\sqrt{1 + \lambda(r, s)^2}$ (see figure 1 and Methods for details). Taking into account the projections of the lift and drag forces onto the rotation plane of the turbine that depend on the apparent velocity, the pitch angle θ_0 , the headwind speed U and the resistive torque C (see again figure 1), \mathbf{M}_a writes

$$\mathbf{M}_a = \frac{3}{2}\rho U^2 \int_0^W \sqrt{1 + \lambda^2} r (C_L(\beta) - \lambda C_D(\beta)) ds \mathbf{e}_z. \quad (3.1)$$

The specific values of lift and drag coefficients were measured separately on a single non-rotating blade. We found the following laws for the coefficients $C_L = 1.49 \cos(\beta) \sin(\beta)$ and $C_D = 0.23 + 1.02 \sin^2(\beta)$ (see Methods). The value of C_P is then obtained by solving numerically the system $M_a = C$ for each set of parameters.

As for experiments, the optimum $C_P(\lambda)$ is a function of the pitch angle θ_0 in the model. Figure 5b shows the ideal efficiency curve $C_P^{\text{opt}}(\lambda)$ (black line) obtained when adapting the pitch angle, following the evolution given in the inset of figure 5b. In addition, we plotted three other standard efficiency curves C_P evaluated at three different constant pitch angles $\theta_0 = 13.8^\circ$, 21.6° and 35.7° . This last result recalls the observation made previously on figure 4, comparing the flexible blades with other rigid cases at different pitch angles. The values of the pitch angle have been chosen such that: (a) the C_P curve matches the optimal distribution for low λ (orange line, $\theta_0 = 35.7^\circ$), (b) the maximum of the C_P curve matches the maximum of the optimal distribution

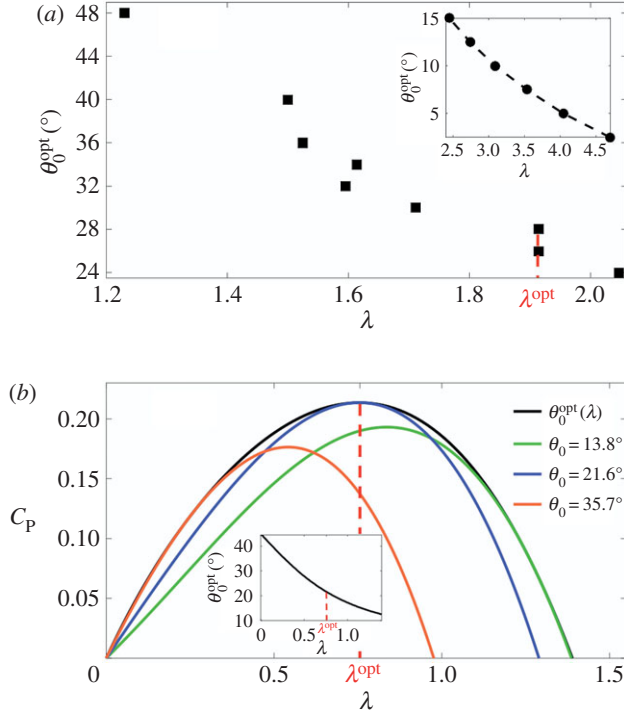


Figure 5. (a) Evolution of the experimental optimal pitch angle θ_0^{opt} as function of the speed ratio λ , showing a decreasing trend over the full working range of the turbine. This trend is confirmed both by commercial wind turbine data [23] (insert) and predictions derived from the model $M_a = C$ (see the text) (insert, figure 5b). (b) Ideal efficiency curve $C_p^{\text{opt}}(\lambda)$ obtained in the model when adapting continually the pitch angle following the evolution given in the insert. In addition, we have plotted three other classic efficiency curves C_p with three different constant pitch angles $\theta_0 = 13.8^\circ, 21.6^\circ, 35.7^\circ$ for comparison. We believe that the quantitative discrepancy between the model and experiments lies in a dependency of drag and lift coefficients with the rotation speed.

(blue line, $\theta_0 = 21.6^\circ$) and (c) the C_p curve matches the optimal distribution for high λ (green line, $\theta_0 = 13.8^\circ$).

Thus, the right strategy to optimize the efficiency curve to changing wind conditions is to adapt the pitch angle from large to small values with increasing λ . Starting from the maximum efficiency C_p^{max} obtained for $\theta_0 = 21.6^\circ$ (blue curve), the pitch angle should decrease to $\theta_0 = 13.8^\circ$ (green curve) for the upper range of λ and increase to $\theta_0 = 35.7^\circ$ (orange curve) for the lower range of λ . This observed decreasing trend of the optimal pitch angle is a general observation for wind turbines: the same trend is confirmed by numerical simulations performed on commercial blade design [23] (displayed in the insert of figure 5a), and by numerical studies [24].

Note that the ranges of $\theta_0^{\text{opt}}(\lambda)$ and λ involved differ between the three representations; reported data for commercial models, for instance, clearly show lower values of optimal pitch angle for higher tip speed ratios λ . As an example the inset of figure 5a shows a turbine model working at λ^{opt} approx. 3.5. This difference lies in the size of the blade and the values of aerodynamic coefficients that differ from one blade design to the other [25–29]. This point has no direct consequence on the discussion, which is essentially based on the decreasing trend of the optimal pitch angle, shared by turbines in general and independent of the blade geometry.

Introducing flexibility to the blades is a way to passively change the pitch angle with working conditions. We shall now address the basis of the reconfiguration mechanisms involved in the enhancement of the production curve C_p . As discussed, θ_0^* must be a decreasing function of λ , or, seen from the maximum working point, must increase if λ decreases and vice versa. For simplicity

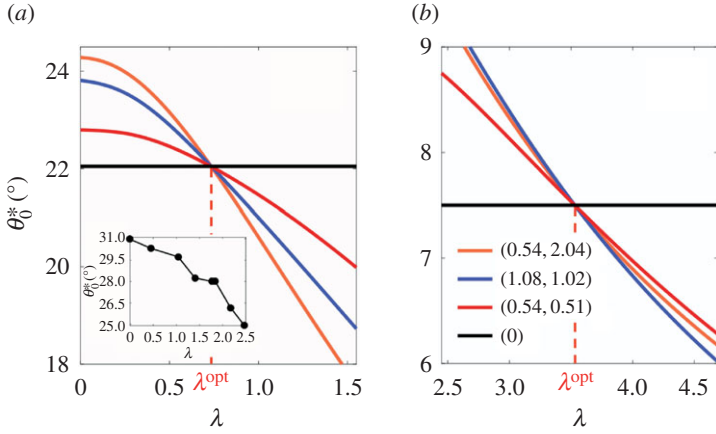


Figure 6. Evolution of the effective pitch angle θ_0^* as a function of the speed ratio λ for (a) aerodynamic coefficients measured in the experiments, $C_L = 1.49 \cos(\beta) \sin(\beta)$ and $C_D = 0.23 + 1.02 \sin^2(\beta)$ (b) aerodynamic coefficients derived from potential flow theory: $C_L = \pi \sin(\beta)$. Black line: rigid case showing a constant pitch angle; red curve ($C_Y = 0.54, C_C = 0.51$) corresponds to experimental parameters; blue curve ($C_Y = 1.08, C_C = 1.02$) corresponds to a softer material where B is divided by two; and orange curve ($C_Y = 0.54, C_C = 2.04$), corresponds to an increased centrifugal term (using a denser material for instance). Black, red, blue and orange curves are obtained for a pitch angle (a) $\theta_0 = 22.05^\circ, 17.89^\circ, 14.02^\circ$ and 19.38° , (b) $\theta_0 = 7.50^\circ, -3.27^\circ, -8.27^\circ$ and 4.07° , respectively. For each curve, the pitch angle θ_0 is tuned in order to get the optimal apparent pitch angle (black line) at λ^{opt} . Here, a constant wind speed U is used for the calculation of each curves. Measurements in experiments of the mean apparent pitch angle at the blade tip are shown in the inset for comparison.

and clarity, this point is addressed here considering a reduced fluid/structure model. In two-dimensional geometry, the elastic blade section may be described using a Euler–Bernoulli beam model [30]. The local forces acting on a section element are (i) the aerodynamic load $\mathbf{f}_L + \mathbf{f}_D$, which tends to fold the blade through the action of the torque \mathbf{m}_a and (ii) the centrifugal force \mathbf{f}_C due to the high rotation rates involved during turbine operation. The component of \mathbf{f}_C locally normal to the blade exerts a torque \mathbf{m}_c in the opposite direction of \mathbf{m}_a , which tends to align the flexible blade with the rotation plane. For a quasisteady approach, the system in dimensionless mathematical form where lengths are normalized by the chord length W writes (see figure 1 and Methods)

$$\frac{\partial^3 \theta}{\partial s^3} = C_Y(1 + \lambda^2)[C_L(\beta(s)) \cos(\beta(s)) + C_D(\beta(s)) \sin(\beta(s))] - C_C \lambda^2 \sin(\theta(s)) \int_0^s \cos(\theta(s')) ds', \quad (3.2)$$

which must satisfy clamped-free boundary conditions $\theta(0) = \theta_s(1) = \theta_{ss}(1) = 0$. C_Y and C_C are respectively referred to as the Cauchy and centrifugal numbers

$$C_Y = \frac{\rho U^2 W^3}{2B} \quad (3.3)$$

and

$$C_C \lambda^2 = \frac{\rho_{blade} \Omega^2 h W^4}{B}. \quad (3.4)$$

C_Y and $C_C \lambda^2$ respectively compare the pressure and centrifugal effects to the elastic restoring force of the bent blade. The pressure load tends to bend the blade towards the headwind and therefore increases the apparent pitch angle ($\theta > \theta_0$), while the role of the centrifugal force is to unfold the blade in the opposite direction ($\theta < \theta_0$). Solutions of equation (3.2) may be easily computed

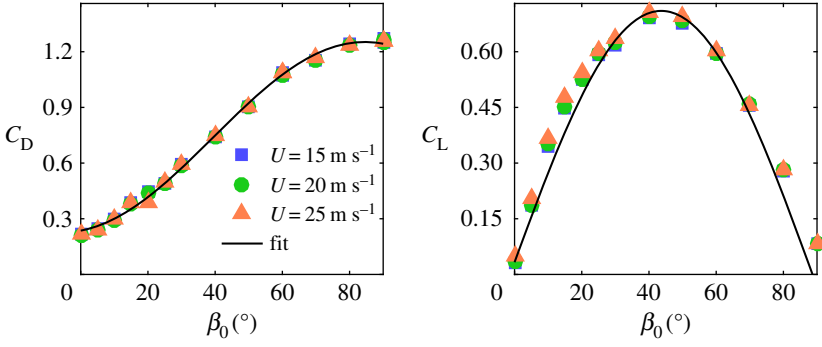


Figure 7. Measurements of macroscopic aerodynamic coefficient $C_D(\beta)$ and $C_L(\beta)$ as a function of the angle of attack β for three different wind speeds. The data are fitted with the following laws: $C_L = 1.49 \cos(\beta) \sin(\beta)$ and $C_D = 0.23 + 1.02 \sin^2(\beta)$ (black lines).

using classical numerical shooting methods. As evoked above, we are interested here in the elastic response of the blade in the vicinity of the optimal working point (defined at $C_p^{\text{opt}}(\lambda^{\text{opt}})$, (figure 5)).

Figure 6a shows the evolution of the average apparent pitch angle $\theta_0^* = \langle \theta(s) \rangle_s$ as a function of λ . For each set of parameters C_Y and C_C , the pitch angle θ_0 is chosen such that the apparent pitch angle $\theta_0^*(\lambda^{\text{opt}})$ at the working point corresponds actually to the optimum pitch angle (θ^{opt}). The red curve represents the case for $C_Y = 0.54$ and $C_C = 0.51$, estimated from experimental values. For the discussion, it is compared to the evolution of $\theta(\lambda)$ for the rigid case (constant angle, black line), a case using a material which is twice as soft (i.e. multiplying C_Y and C_C by a factor of 2, $C_Y = 1.08$, $C_C = 1.02$), and a case only amplifying the centrifugal effect ($C_Y = 0.54$, $C_C = 2.04$). As can be seen, equation (3.2) leads to a decreasing apparent pitch angle in the vicinity of the working point, which corresponds to the desired effect for performance improvement as discussed above.

The results also pinpoint the importance of both C_Y and C_C in tuning the elastic response of the flexible blades. For instance, decreasing the blade stiffness and/or increasing the centrifugal effects sharpen the evolution of θ_0^* in the vicinity of the optimal working point, which allows the flexible blade to explore a larger range of angle of attack. This represents an interesting deciding point for turbine blades design: the response of the elastic blade can be finely tuned with flexibility and centrifugal contributions by changing blade parameters such as density, Young modulus, or thickness. Such key parameters should be chosen carefully to impose the elastic law as close as possible to the optimal curve $\theta_0^{\text{opt}}(\lambda)$. Hence, an elastic law covering an insufficient range of θ_0^* will not be efficient. Reciprocally, covering an excessively large range (choosing a excessively flexible material, as in the case F_2 for instance), will cause the performance to collapse.

Finally, we observe that this beneficial evolution of the elastic behaviour of the blades still holds if the form of the aerodynamical laws are changed. Figure 6b shows the same results as figure 6a when considering aerodynamic coefficients derived, this time, from foil potential flow theory at small angle of attack: $C_L = \pi \sin(\beta)$ [25]. This theory is often used for large and profiled wind turbine blades operating at high λ [1], then involving small angles β and pre-stall (potential) flows. Again, the apparent pitch angle decreases with λ in the vicinity of the optimum, strengthening the benefit of using flexible blades in general.

4. Conclusion

Our experiments showed significant energy gain (approx. 35%) compared with its rigid counterpart. With self-adaptation to wind conditions, this system enlarges the range of wind speeds for which the machine works properly, feature obtained with non-consuming mechanisms. Moreover, the small magnitudes of the deformations involved may also be worthwhile for manufacturing issues.

The mechanisms described here do not depend, *a priori*, on the blade design and only require that the optimal pitch angle is a decreasing function of λ . As seen, the full reconfiguration mechanisms require both fluid pressure and centrifugal forces for a proper evolution of the apparent pitch angle θ_0^* with λ . This can be achieved by tuning carefully the terms C_C and C_Y , with the density, flexibility and geometry of the blade. Finally, we believe that the advantages of using flexible blades may extend beyond the scope of this paper. This work mainly focused on steady, time-independent regimes. However, the blades capability to redirect the torque via the chordwise bending may certainly be beneficial for the dynamical response, and helps the rotor to adapt to intermittency and optimizes energy conversion. We anticipate that propellers as used for helicopters or drones would also benefit from using flexible blades through the mechanisms exposed in this article.

5. Methods

(a) Experimental set-up

Blades are rectangular Mylar plates of length $L = 10$ cm and chord $W = 4.5$ cm, clamped along their length to a 1 cm diameter rigid cylinder attached to the rotor. The part of the blade's chord that can deform is thus 3.5 cm wide. The tip of the blade is 14.6 cm far from the centre of the rotor. The blades flexural rigidity B per unit length is varied using different plate thicknesses h . For each blade, the pitch angle θ_0 is known with an uncertainty of one degree. Finally, particular attention was paid to the mechanical friction of the rotor, using precision machine work and high-quality bearings.

The value of B is measured via the first resonant mode frequency of each blade using a high precision shaker. Following simple beam vibration theory [31], the relation between flexural rigidity and resonant frequency is written

$$f_1 = \frac{1}{2\pi} \left(\frac{1.8751}{W} \right)^2 \sqrt{\frac{B}{\rho h}}, \quad (5.1)$$

where ρ is the density of the Mylar (1380 kg m^{-3}) and 1.8751 is a characteristic coefficient of the first resonant mode. The bending modulus of F_1 and F_2 are $B_1 = 8.41 \cdot 10^{-3} \text{ N m}$ and $B_2 = 1.52 \cdot 10^{-3} \text{ N m}$.

Experiments were carried out in a large wind tunnel of 1.65×1.35 m rectangular cross section. The wind speeds range from 0 to 20 m s^{-1} with a turbulence rate of 0.5%. A magnetic powder brake generates a resisting torque C on the rotor, which ranges from 7 to 175 mN m. The (U, C) plane has been fully explored experimentally, as shown in figure 2.

Both lift and drag forces F_L and F_D for $\Omega = 0$ were measured on a single blade using a mechanical two-component force gauge sensor, varying the angle of attack β with respect to the oncoming wind from 0 to 90° for three different wind speeds. Macroscopic lift and drag coefficients C_L and C_D are calculated using the relation

$$C_{L/D}(\beta) = \frac{2F_{L/D}(\beta)}{\rho_{\text{air}} U^2 S}, \quad (5.2)$$

where ρ_{air} is the density of air, U the velocity of the oncoming wind, measured with a Pitot tube probe ahead of the turbine, and S the total area of the blade $L \times W$.

(b) Model

(i) Expression of the aerodynamic torque

The total aerodynamic torque M_a exerted on a blade section dr by the fluid is estimated by integrating local contributions dM_a on a surface element $d^2S = ds dr$. For a three-bladed model, this expression, per unit length, is written (for $r \gg s$) $\mathbf{M}_a = 3 \int_0^W d\mathbf{M}_a$, which gives the following

expression for \mathbf{M}_a (figure 1)

$$\frac{3\rho}{2} \int_0^W V^2 r (C_L(\beta, r) \sin(\phi) - C_D(\beta, r) \cos(\phi)) d\mathbf{s} \mathbf{e}_z, \quad (5.3)$$

where $C_L(\beta, r)$ and $C_D(\beta, r)$ are local expressions of force coefficients that we assume to be equal to the measured macroscopic coefficients. Following figure 1, it is easy to show that $V^2 = U^2(1 + \lambda^2)$ and $\cos(\phi) = \lambda/(1 + \lambda^2)$; $\sin(\phi) = 1/(1 + \lambda^2)$, which gives the expression of equation (3.1), taking into account local expression of $\lambda = r\Omega/U$.

(ii) Expression of the centrifugal term

The centrifugal force applied on a surface element $d^2S = ds dr$ is

$$\mathbf{f}_c = \rho_{\text{blade}} h \Omega^2 \mathbf{H} \mathbf{M}(s, r), \quad (5.4)$$

where M indicates the blade element on which the centrifugal force applies, and H the orthogonal projection of M on the rotor axis. As the pitch angle is non-zero, vector $\mathbf{H} \mathbf{M}$ has a component normal to the blade. For the blade deformation, bending chordwise, we are only interested in the normal projection, which is at $M(r, s)$

$$f_{c\perp} = \rho_{\text{blade}} h W \Omega^2 \sin(\theta_0^*(s)) \int_0^s \cos(\theta_0^*(s')) ds'. \quad (5.5)$$

(iii) Solution of the Euler–Bernoulli beam equation

Solutions of equation (3.2), involving the bent shape of the flexible blades for each set of parameters ($\lambda, B, \theta_0, C_D, C_L$), were obtained numerically using classic numerical routines. The exact shape is calculated by solving the nonlinear clamped/free Euler–Bernoulli equation using a shooting method routine. The blade is discretized with 5000 points along the chord giving a sufficient precision for convergence of the efficiency $C_P(B, \theta_0, \lambda)$.

Authors' contributions. V.C. performed the experiments, analysed the data, wrote the paper and participated in discussing and approving the final version of the paper. S.C.d.P. analysed the data, wrote the paper, participated in discussing and approving the final version of the paper, conceived and directed the project. I.D. and F.M. helped in the design of the experiment in the wind tunnel. B.T. analysed the data, drafted the first version of the manuscript, wrote the paper, participated in discussing and approving the final version of the paper, conceived and directed the project.

Competing interests. We have no competing interests.

Funding. There is no funding to report for this submission.

Acknowledgements. We are grateful to S. Tardy and L. Tuckerman for their careful reading of the manuscript. We thank A. Di Palma, F. Filaine, L. Rea and M. Receveur for technical assistance.

References

1. Hansen MOL. 2015 *Aerodynamics of wind turbines*. London, UK: Routledge.
2. Schubel PJ, Crossley RJ. 2012 Wind turbine blade design. *Energies* **5**, 3425–3449. (doi:10.3390/en5093425)
3. Castagnet D, Barlas T, Buhl T, Poulsen N, Wedel-Heinen J, Olesen N, Bak C, Kim T. 2014 Full-scale test of trailing edge flaps on a Vestas V27 wind turbine: active load reduction and system identification. *Wind Energ.* **17**, 549–564. (doi:10.1002/we.1589)
4. Schouveiler L, Boudaoud A. 2006 The rolling up of sheets in a steady flow. *J. Fluid Mech.* **563**, 71–80. (doi:10.1017/S0022112006000851)
5. Alben S, Shelley M, Zhang J. 2002 Drag reduction through self-similar bending of a flexible body. *Nature* **420**, 479–481. (doi:10.1038/nature01232)
6. Shelley MJ, Zhang J. 2011 Flapping and bending bodies interacting with fluid flows. *Annu. Rev. Fluid Mech.* **43**, 449–465. (doi:10.1146/annurev-fluid-121108-145456)
7. Vogel S. 1989 Drag and reconfiguration of broad leaves in high winds. *J. Exp. Bot.* **40**, 941–948. (doi:10.1093/jxb/40.8.941)

8. de Langre E. 2008 Effects of wind on plants. *Annu. Rev. Fluid Mech.* **40**, 141–168. (doi:10.1146/annurev.fluid.40.111406.102135)
9. Gosselin F, de Langre E, Machado-Almeida BA. 2010 Drag reduction of flexible plates by reconfiguration. *J. Fluid Mech.* **650**, 319–341. (doi:10.1017/S00222112009993673)
10. Thiria B, Godoy-Diana R. 2010 How wing compliance drives the efficiency of self-propelled flapping flyers. *Phys. Rev. E* **82**, 015303. (doi:10.1103/PhysRevE.82.015303)
11. Ramananarivo S, Godoy-Diana R, Thiria B. 2011 Rather than resonance, flapping wing flyers may play on aerodynamics to improve performance. *Proc. Natl Acad. Sci. USA* **108**, 5964–5969. (doi:10.1073/pnas.1017910108)
12. Marais C, Thiria B, Wesfreid JE, Godoy-Diana R. 2012 Stabilizing effect of flexibility in the wake of a flapping foil. *J. Fluid Mech.* **710**, 659–669. (doi:10.1017/jfm.2012.390)
13. Jureczko M, Pawlak M, Mezyk A. 2005 Optimisation of wind turbine blades. *J. Mater. Process. Technol.* **167**, 463–471. (doi:10.1016/j.jmatprotec.2005.06.055)
14. Ponta FL, Otero AD, Lago LI, Rajan A. 2016 Effects of rotor deformation in wind-turbine performance: the dynamic rotor deformation blade element momentum model (DRD–BEM). *Renewable Energy* **92**, 157–170. (doi:10.1016/j.renene.2016.01.098)
15. Motley MR, Liu Z, Young YL. 2009 Utilizing fluid–structure interactions to improve energy efficiency of composite marine propellers in spatially varying wake. *Composite Struct.* **90**, 304–313. (doi:10.1016/j.compstruct.2009.03.011)
16. Hoogendoorn E, Jacobs GB, Beyene A. 2010 Aero-elastic behavior of a flexible blade for wind turbine application: a 2d computational study. *Energy* **35**, 778–785. (doi:10.1016/j.energy.2009.08.030)
17. Puterbaugh M, Beyene A. 2011 Parametric dependence of a morphing wind turbine blade on material elasticity. *Energy* **36**, 466–474. (doi:10.1016/j.energy.2010.10.018)
18. MacPhee D, Beyene A. 2011 A flexible turbine blade for passive blade pitch control in wind turbines. In *2011 IEEE Power Engineering and Automation Conference (PEAM 2011)*, Wuhan, China, 8–9 September, vol. 1, pp. 196–199. Piscataway, NJ: IEEE.
19. Krawczyk P, Beyene A, MacPhee D. 2013 Fluid structure interaction of a morphed wind turbine blade. *Int. J. Energy Res.* **37**, 1784–1793. (doi:10.1002/er.2991)
20. MacPhee DW, Beyene A. 2015 Experimental and fluid structure interaction analysis of a morphing wind turbine rotor. *Energy* **90**, 1055–1065. (doi:10.1016/j.energy.2015.08.016)
21. MacPhee DW, Beyene A. 2016 Fluid–structure interaction analysis of a morphing vertical axis wind turbine. *J. Fluids Struct.* **60**, 143–159. (doi:10.1016/j.jfluidstructs.2015.10.010)
22. Franco JA, Jauregui JC, Toledano-Ayala M. 2015 Optimizing wind turbine efficiency by deformable structures in smart blades. *J. Energy Resour. Technol.* **137**, 051206–051206. (doi:10.1115/1.4030445)
23. Burton T, Sharpe D, Jenkins N, Bossanyi E. 2001 *Wind energy handbook*. New York, NY: J. Wiley & Sons.
24. Lanzafame R, Messina M. 2007 Fluid dynamics wind turbine design: critical analysis, optimization and application of BEM theory. *Renewable Energy* **32**, 2291–2305. (doi:10.1016/j.renene.2006.12.010)
25. Abbott IH, Von Doenhoff AE. 1959 *Theory of wing sections, including a summary of airfoil data*. North Chelmsford, MA: Courier Corporation.
26. Timmer WA. 2010 Aerodynamic characteristics of wind turbine blade airfoils at high angles-attack. In *3rd EWEA Conference Torque 2010: The Science of Making Torque from Wind*, Heraklion, Crete, Greece, 28–30 June. Brussels, Belgium: European Wind Energy Association.
27. Timmer WA, van Rooij RPJOM. 2003 Summary of the Delft University wind turbine dedicated airfoils. *J. Sol. Energy Eng.* **125**, 488–496. (doi:10.1115/1.1626129)
28. Herráez I, Stoevesandt B, Peinke J. 2014 Insight into rotational effects on a wind turbine blade using Navier–Stokes computations. *Energies* **7**, 6798–6822. (doi:10.3390/en7106798)
29. Tangler J, Kocurek D. 2005 Wind turbine post-stall airfoil performance characteristics guidelines for blade-element momentum methods. In *43rd AIAA Aerospace Sciences Meeting and exhibit*, Reno, Nevada, 10–13 January. Reston, VA: American Institute of Aeronautics and Astronautics.
30. Landau LD, Lifshitz EM. 1970 *Theory of elasticity*, 2nd English edition. Course of Theoretical Physics, vol. 7. Oxford, UK: Pergamon Press.
31. Thomson W. 1996 *Theory of vibration with applications*. Boca Raton, FL: CRC Press.